Supplementary materials

Template Assisted *In Situ* Synthesis of Ag@Au Bimetallic Nanostructures Employing Liquid Phase Transmission Electron Microscopy

Nabeel Ahmad, [a*] *Marta Bon,* [a*] *Daniele Passerone,* [b] *Rolf Erni* [a]

a) Electron Microscopy Center, Empa, Überlandstrasse 129, CH-8600, Dübendorf.

b) nanotech@surfaces, Empa, Überlandstrasse 129, CH-8600, Dübendorf

*) The two authors equally contributed to the work.

Table of Contents

S.1 Experimental Evidence

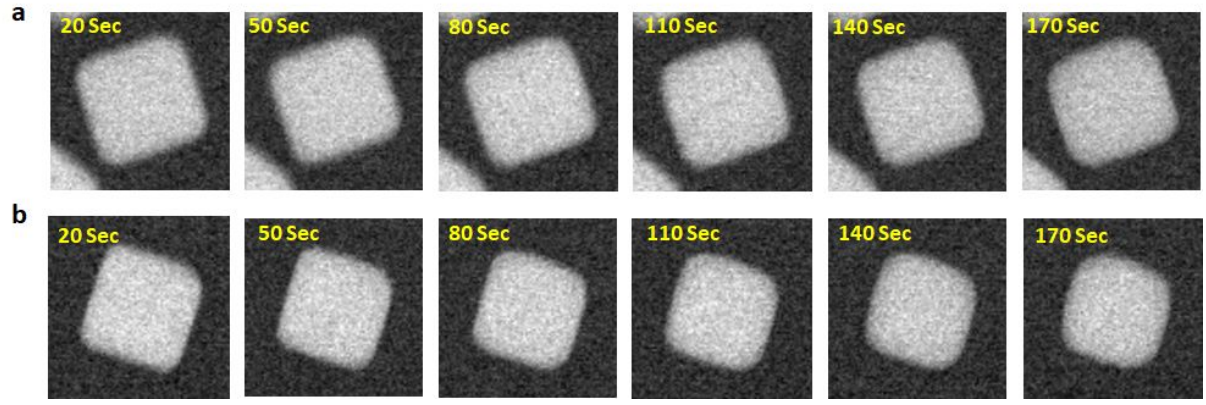

Fig. S1. Dissolution behavior of Ag nanocubes under the beam while encapsulated in DMA. (a) *STEM-HAADF images in methanol solvent with 200mM DMA concentration showing slowdown of etching under electron beam of Ag nanocubes at* $\dot{d}$ *= 20.0 electrons/Å*^{2}*s.* ***(b)*** *Etching of nanocube in 50mM of DMA at similar* $\dot{d}$ *= 20.0 electrons/Å*^{2}*s.*

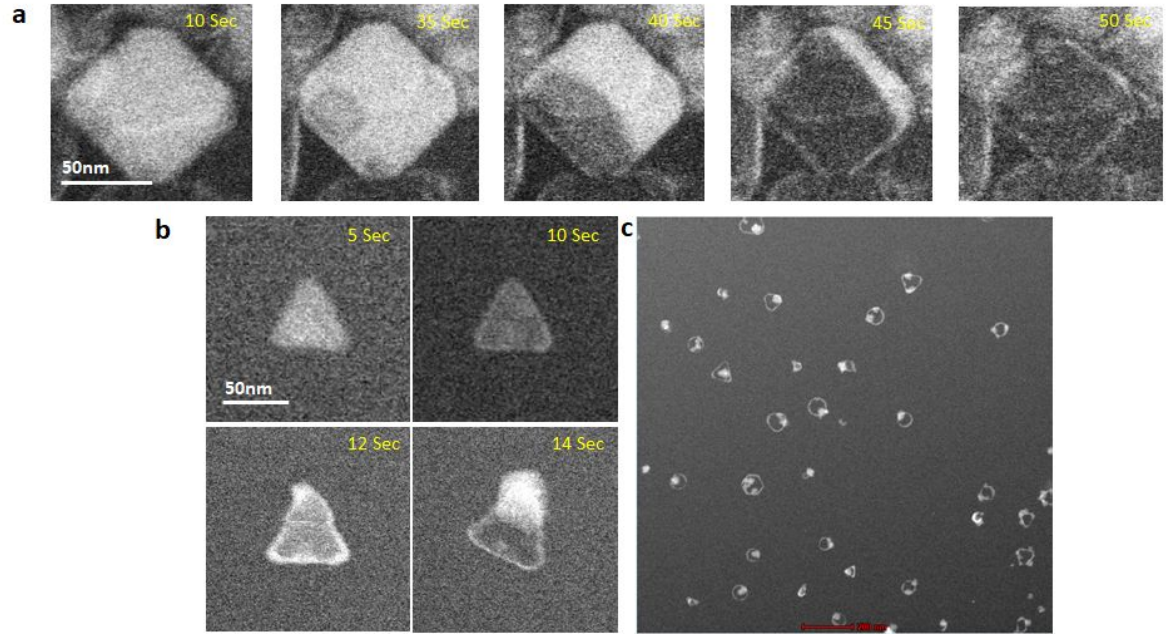

Fig. S2. Galvanic replacement reactions on Ag nanoparticle templates. (a) *STEM-HAADF images in methanol solvent showing hollowing out of of nanocube at* $\dot{d}$ *= 5.0 electrons/Å*^{2}*s.* ***(b)*** *Time resolved series of images of triangular nanoplate hollowed out leaving behind a thin frame of Au rich alloy at edges.* ***(c)*** *Low magnification image showing several hollow hexagonal and triangular nanoplates.*

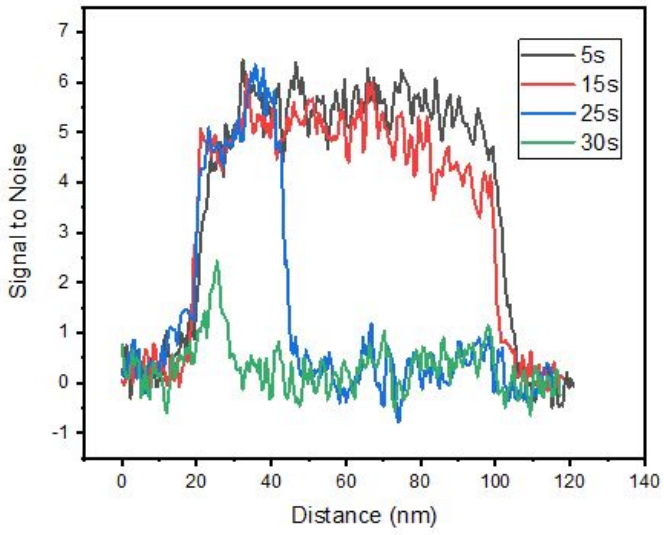

Fig. S3. Line plot for nanocube in Fig S2*. Galvanic replacement reactions at* $\dot{d}$ *= 5.0 electrons/Å*^{2}*s in methanol and 100μM of* $HAuCl_4$ *showing the complete hollowing out of the nanocube in under 40 seconds.*

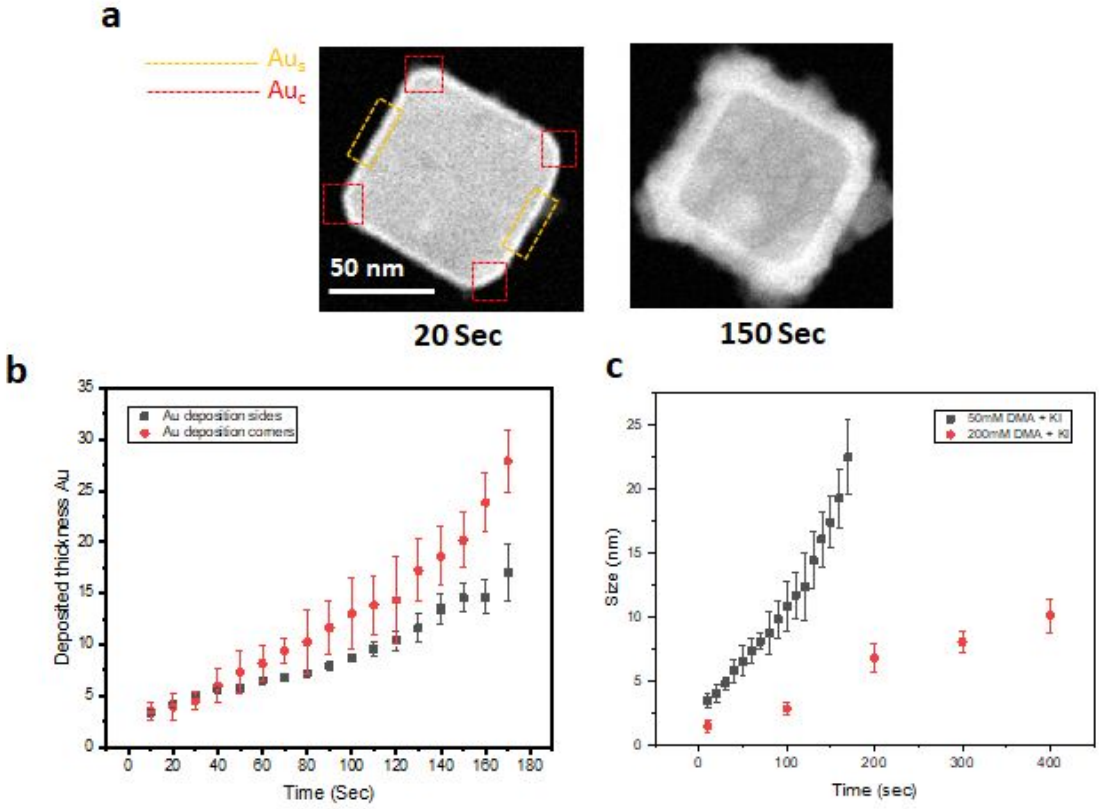

Fig. S4. STEM-HAADF images showing comparison of deposition at corner and sides of nanocube at initial and later stages of growth. (a) *Au deposition after first 20 seconds of beam irradiation* $\dot{d}$ *= 20.0 electrons/Å*^{2}*s and subsequently 150 seconds.* ***(b)*** *Plot comparing deposition of Au at corner vs*

sides of cube, comparing average deposition thickness of Au at various growth stages in 50mM DMA +KI. ***(c)*** *Comparison of overall growth profile in 50mM DMA + KI vs 200MM DMA + KI.*

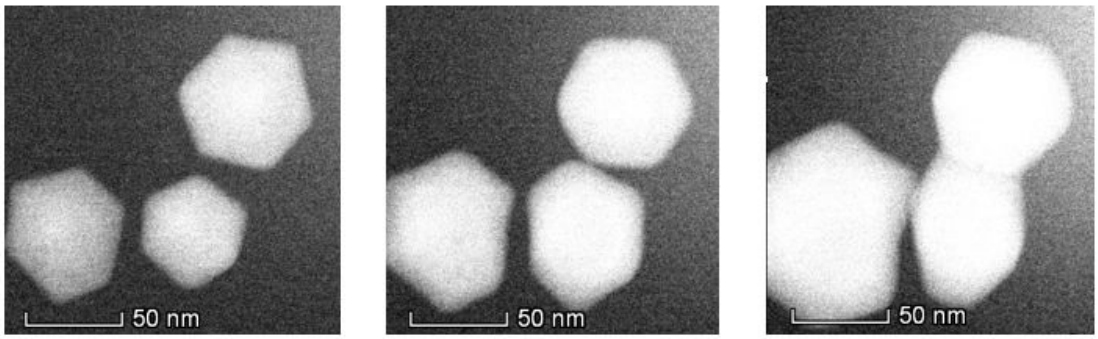

Fig. S5. HAADF Images showing growth and subsequent ripening of nanoplates under high dose exposure for EDX mapping in DMA without supply of $HAuCl_4$.

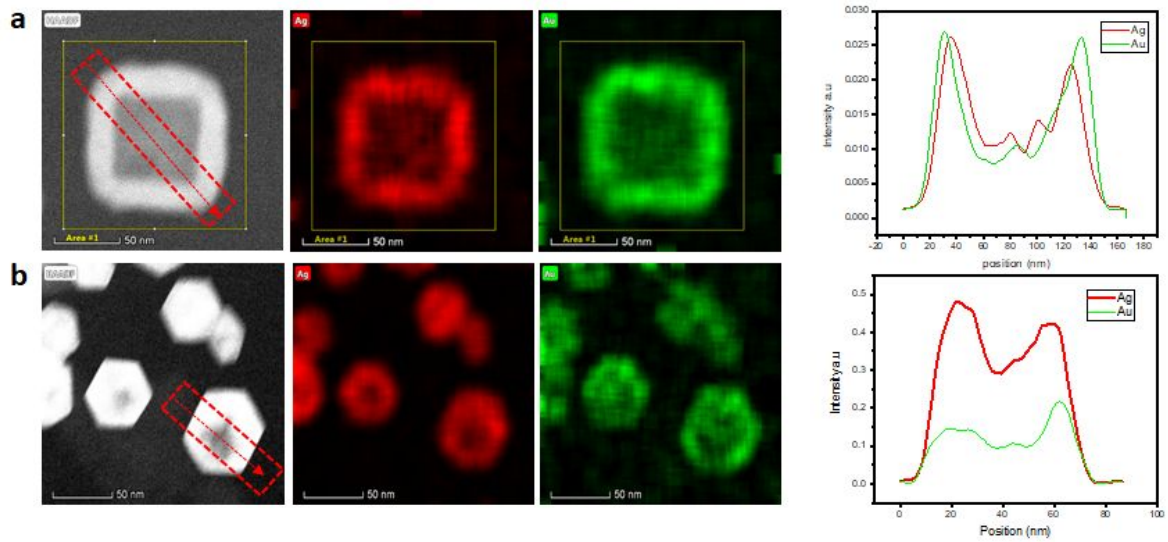

Fig. S6. HAADF and elemental Distribution maps of Ag@Au grown in methanol and DMA. (a) *Partially hollow Ag@Au nanocube along with its associated intensity profile showing that Ag has mostly diffused towards the edges of the cubic profile.* ***(b)*** *Bimetallic nanoplates in DMA showing similar partial hollowing out effect in the presence of DMA which is markedly visible in the intensity profile however the Au content is lower than in the case of cubic nanoparticles.*

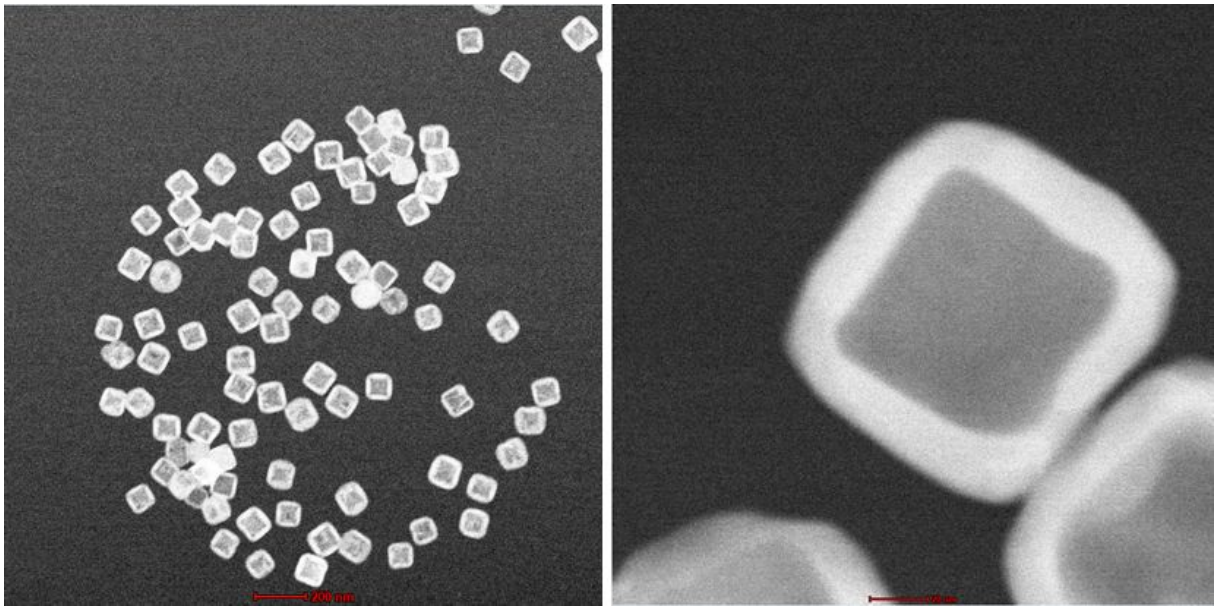

Fig. S7. HAADF-STEM image of partially hollow Ag@Au naoparticles synthesized in solution containing methanol and DMA.

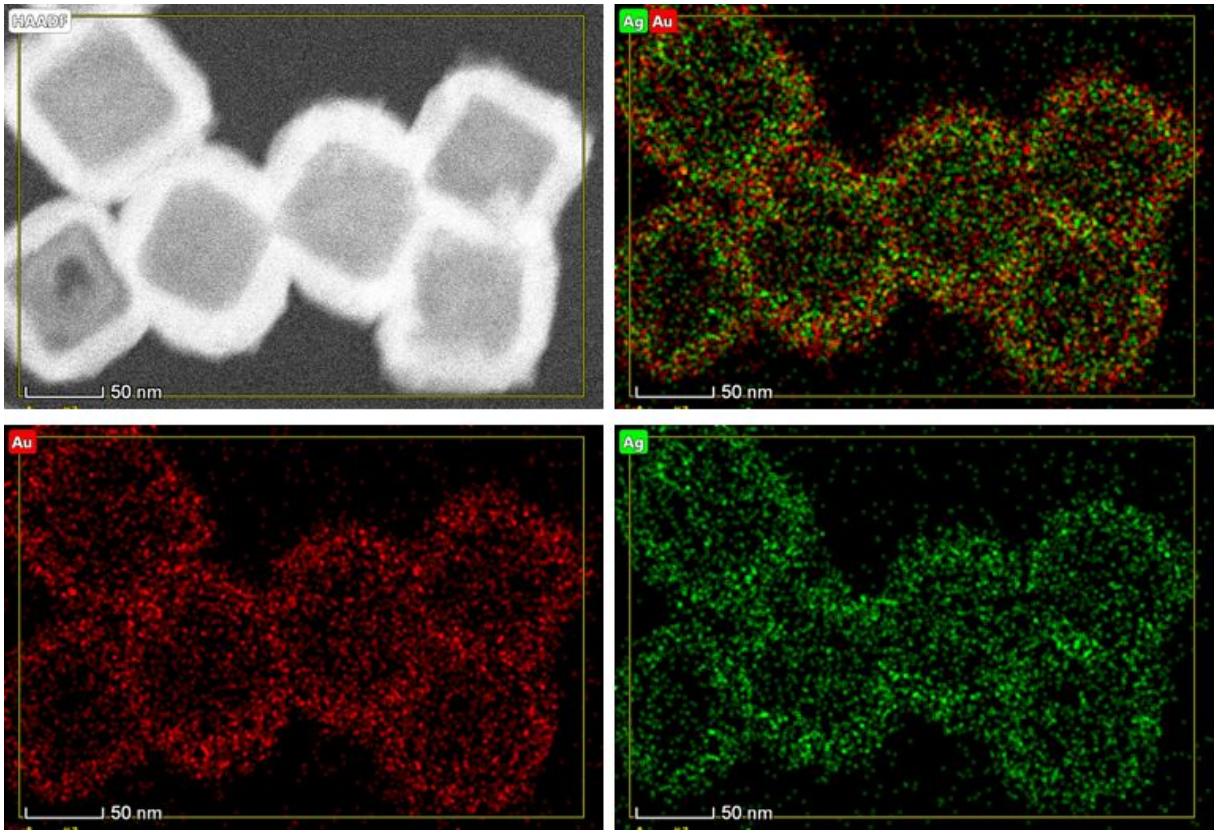

Fig. S8. HAADF and elemental Distribution maps of Ag@Au grown in methanol and DMA. *Several partially hollow Ag@Au core-shell naoparticles showing the overlapped as well as separate distribution of Au and Ag.*

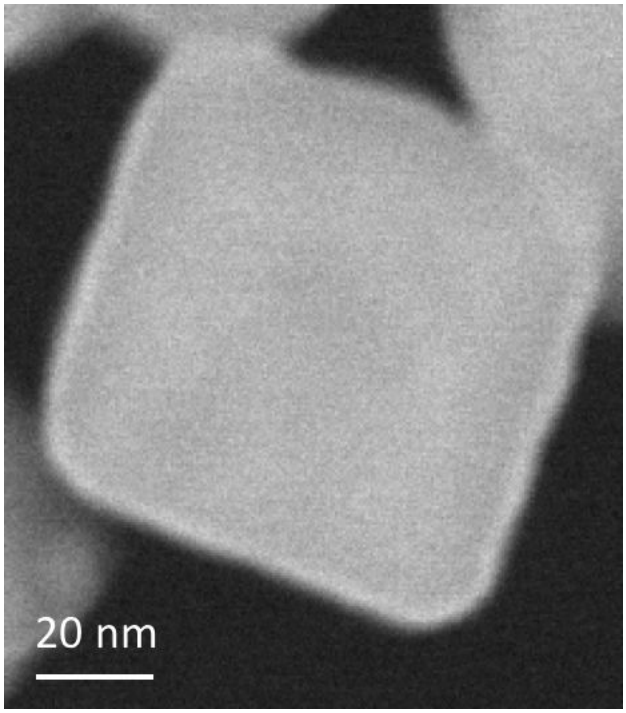

Fig. S9. High magnification image of nanocube showing clearly the thin epitaxial layer of Au over Ag in 200mM DMA and KI.

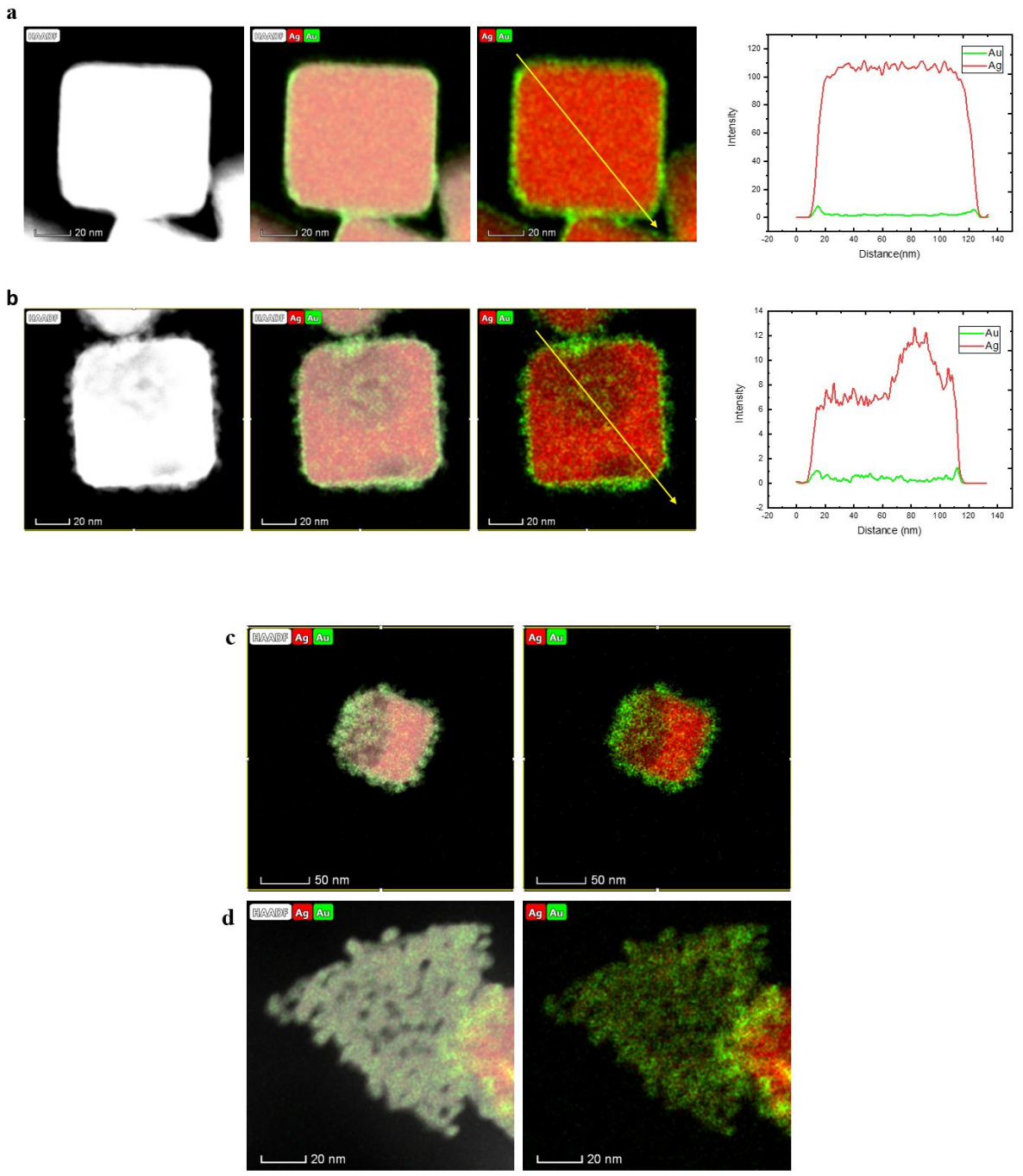

Fig. S10. HAADF and elemental Distribution maps of Ag@Au nanostructures ex situ. (a) *Ag@Au nanocubes after 2 hrs in 0.5mM $HAuCl_4$ +DMA, KI along with associated line profile. Partially hollow Ag@Au nanocubes after 2 hrs in 0.5mM $HAuCl_4$ with associated line plot. (c&d) Partially hollow Ag@Au nanocubes and nanoplate after 4 hrs in 0.5mM $HAuCl_4$.*

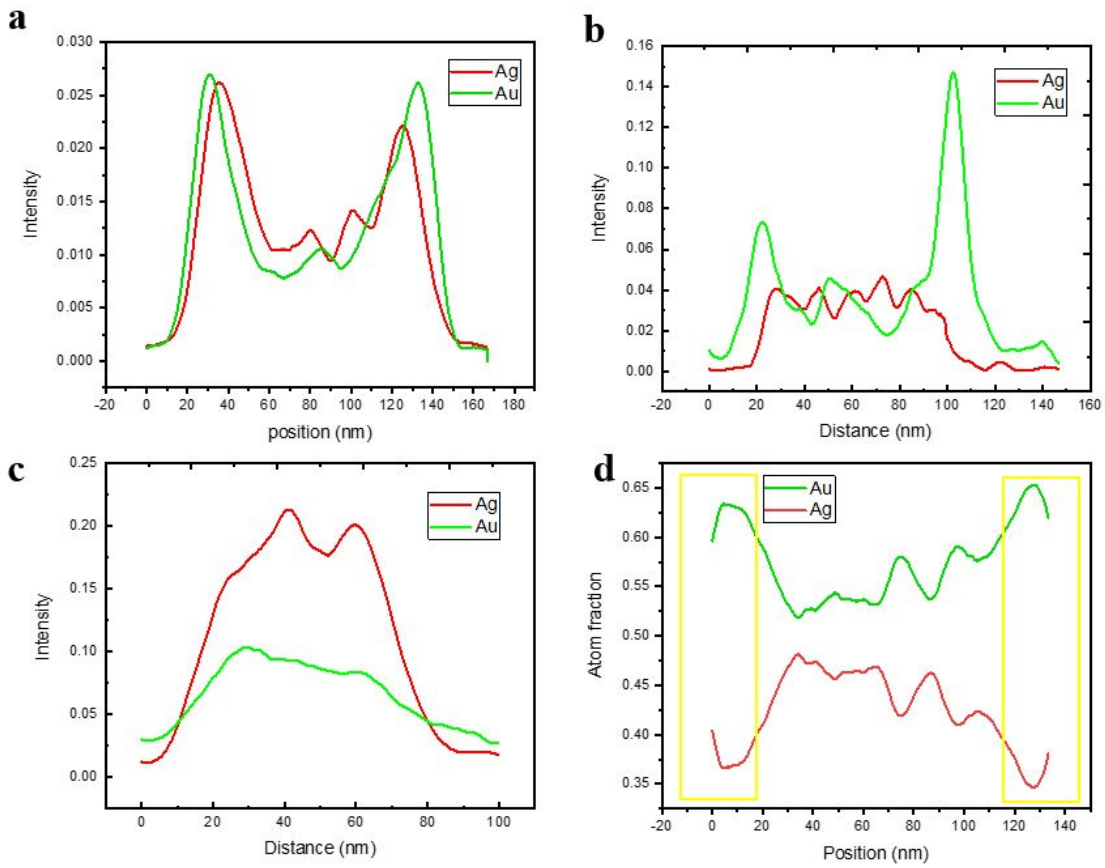

Fig. S11. Intensity profiles of Au and Ag from EDX mapping in situ*. (a) Profile of Ag@Au nanocube in presence of DMA only. (b) Line profile of Ag and Au for the case of nanocube in DMA +KI. (c) Line profile of Ag and Au for the case of Ag@Au nanoplate in DMA+KI. (d) Atom fraction profile from Ag@Au nanocube for (a).*

S.2 Simulations

S.2.3 Ab-initio Structural Optimizations: DMA on Ag low-index surfaces.

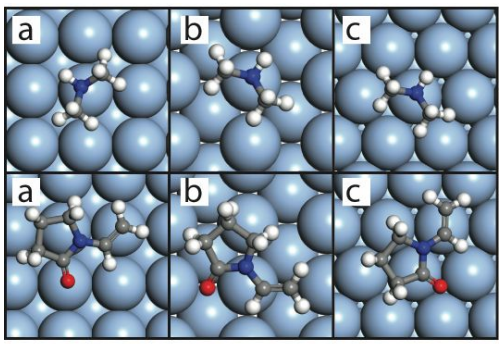

Fig. S12. Adsorption energies of two different molecules on three low index Ag surfaces, i.e. (100), (110) and (111). Upper panel: Dimethylamine (DMA). Bottom Panel: 2-pyrollidone (2P), building block for the polyvinyl pyridine (PVP). Molecules are shown in ball&stick representation, with the

following color-scheme: gray) carbon, red) oxygen, blue) nitrogen, white) hydrogen. The substrate is shown with van der Waals spheres and is colored in light blue.

S.2.1 Classical Molecular Dynamics: Comparison between two commonly used Embedded Atom Models

In the following we report the comparison between the molecular dynamics simulations of the Au deposition on the cubic Ag seed, as obtained by using two different force-fields for the parametrization of the Ag-Au interactions, i.e. the EAM-Foiles[1] and the EAM-Zhou.[2] Data reported are obtained at 300 K with Au deposition stride equal to 2 fs.

As shown in Fig. S14, the EAM-Zhou predicts a greater number of Au atoms inside the nanoparticle (NP) compared to EAM-Foiles. This is due to the fact that the energy barriers for processes leading to the intermixing of the species (mainly in-channel diffusion) estimated by EAM-Zhou are lower compared to the ones by EAM-Foiles (and by ab-initio estimations).[3]

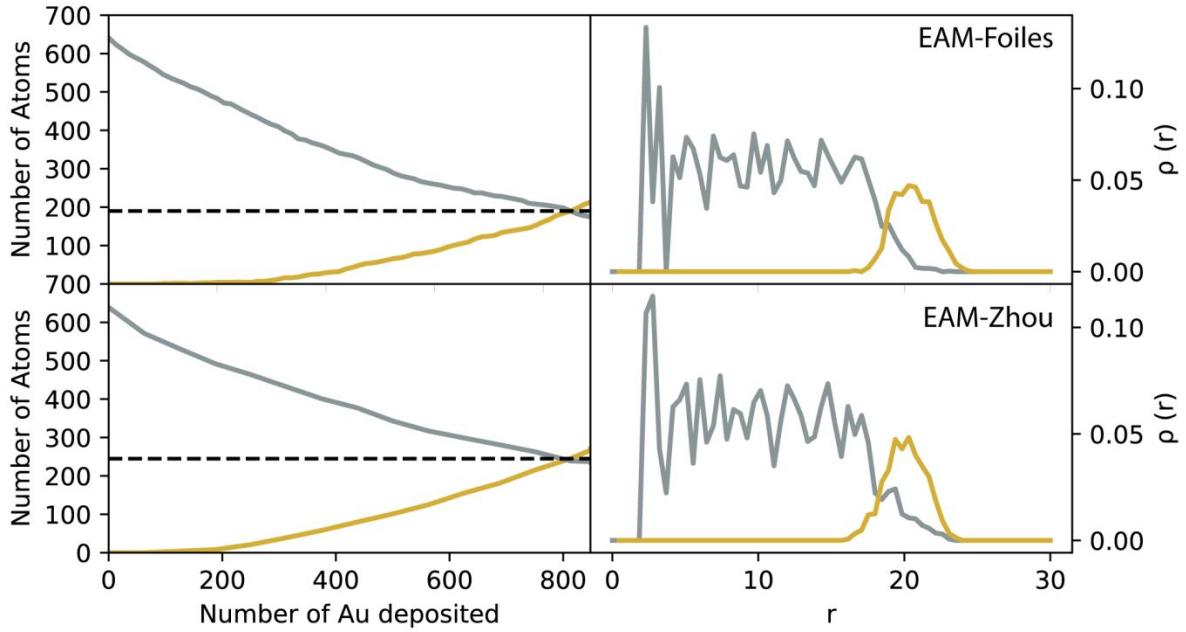

Fig. S14. Surface analysis during the nanoalloy growth resulting from MD simulations with two EAMs, i.e. EAM-Foiles (upper panel)[1] and EAM-Zhou (bottom panel).[2] Left) *Number of Ag atoms (silver curve) at the surface and number of Au atoms (gold curve) inside the NP.* ***Right)*** *Radial distribution functions of the last 5 equilibrated ns of $Ag_N@Au_{N/2}$ NP as function of the distance r from the NP center. Data obtained for the cubic NP at 300 K with Au deposition stride equal to 2 fs.*

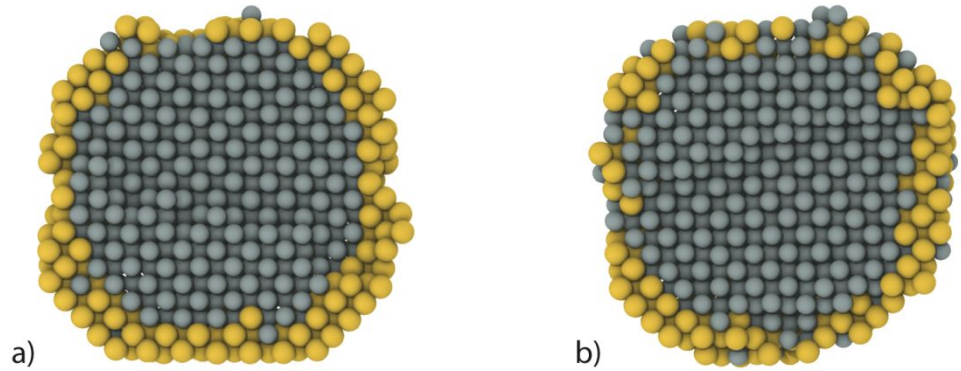

Fig. S15. Cross-sectional view of final configuration for the cubic nanoparticle, as obtained by using EAM-Foiles (a) and EAM-Zhou (b). *Data obtained for the cubic NP at 300 K with Au deposition stride equal to 2 fs.*

S.2.1 Classical Molecular Dynamics: Comparison between different temperatures and deposition strides.

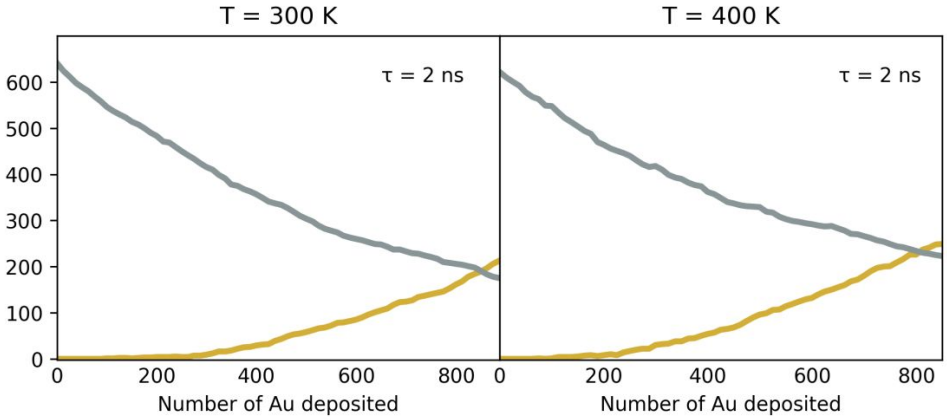

Fig. S16 Surface analysis during the nanoalloy growth resulting from MD simulations at two different temperatures.

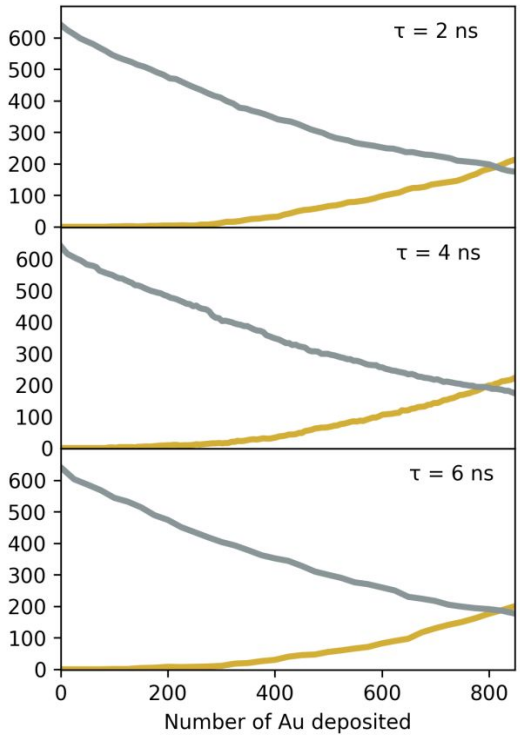

Fig. S17. Surface analysis during the nanoalloy growth resulting from MD simulations at two different temperatures. *Data shown are obtained at T=300 K.*

As shown in Figs. S16 and S17 we did not recover any significant difference in the properties discussed in the manuscript (i.e. surface defects, radial distribution function and final shape of the NP) depending on temperature and deposition strides.

References

(1) Foiles, S. M.; Baskes, M. I.; Daw, M. S. Embedded-Atom-Method Functions for the Fcc Metals Cu, Ag, Au, Ni, Pd, Pt, and Their Alloys. *Phys. Rev. B* **1986**, *33*, 7983–7991.

(2) Zhou, X. W.; Johnson, R. A.; Wadley, H. N. G. Misfit-Energy-Increasing Dislocations in Vapor-Deposited CoFe/NiFe Multilayers. *Phys. Rev. B - Condens. Matter Mater. Phys.* **2004**, *69*, 1–10.

(3) Bon, M.; Ahmad, N.; Erni, R.; Passerone, D. Reliability of Two Embedded Atom Models for the Description of Ag@Au Nanoalloys. *J. Chem. Phys.* **2019**, *151*, 064105.